Molecular modeling of Trypanosoma cruzi glutamate cysteine ligase and investigation of its interactions with glutathione

ARTICLE *in* JOURNAL OF MOLECULAR MODELING · SEPTEMBER 2011

Impact Factor: 1.74 · DOI: 10.1007/s00894-011-1224-z · Source: PubMed

6 AUTHORS, INCLUDING:

Carlos F. Lagos
Pontifical Catholic University of Chile
40 PUBLICATIONS **125** CITATIONS
SEE PROFILE

Raul Araya-Secchi
The Ohio State University
12 PUBLICATIONS **55** CITATIONS
SEE PROFILE

Tomas Perez-Acle
Fundación Ciencia Para la Vida
47 PUBLICATIONS **546** CITATIONS
SEE PROFILE

Cristian O Salas
Pontifical Catholic University of Chile
42 PUBLICATIONS **258** CITATIONS
SEE PROFILE

J Mol Model (2012) 18:2055–2064
DOI 10.1007/s00894-011-1224-z

ORIGINAL PAPER

Molecular modeling of *Trypanosoma cruzi* glutamate cysteine ligase and investigation of its interactions with glutathione

Carlos F. Lagos · Raul Araya-Secchi · Pablo Thomas · Tomás Pérez-Acle · Ricardo A. Tapia · Cristian O. Salas

Received: 17 June 2011 / Accepted: 11 August 2011 / Published online: 6 September 2011

Abstract *Trypanosoma cruzi* glutamate cysteine ligase (TcGCL) is considered a potential drug target to develop novel antichagasic drugs. We have used a variety of computational methods to investigate the interactions between TcGCL with Glutathione (GSH). The three-dimensional structure of TcGCL was constructed by comparative modeling methods using the *Saccharomyces cerevisiae* glutamate cysteine ligase as template. Molecular dynamics simulations were used to validate the TcGCL model and to analyze the molecular interactions with GSH. Using RMSD clustering, the most prevalent GSH binding modes were identified paying attention to the residues involved in the molecular interactions. The GSH binding modes were used to propose pharmacophore models that can be exploited in further studies to identify novel antichagasic compounds.

Keywords Comparative modeling · Glutamate cysteine ligase · Molecular dynamics · Pharmacophore · *Trypanosoma cruzi*

Introduction

Chagas disease represents the leading cause of cardiac lesions in young, economically productive adults in Latin American countries where this disease is endemic [1]. *Trypanosoma cruzi*, the eukaryotic protozoan responsible for Chagas disease, has a redox metabolism based on trypanothione, a glutathionyl spermidine derivative. In *Trypanosoma cruzi*, glutathione (GSH) is synthesized from its constituent amino acids by the consecutive actions of

Carlos F. Lagos and Raul Araya-Secchi have contributed equally to this work.

Electronic supplementary material The online version of this article (doi:10.1007/s00894-011-1224-z) contains supplementary material, which is available to authorized users.

C. F. Lagos
Departamento de Farmacia, Facultad de Quimica,
P. Universidad Catolica de Chile,
Av Vicuña Mackenna 4860,
Macul-Santiago, Chile

C. F. Lagos · R. Araya-Secchi
Departamento de Ciencias Biologicas, Facultad de Ciencias Biologicas, Universidad Andres Bello,
Av Republica 217,
Santiago, Chile

R. Araya-Secchi · T. Pérez-Acle
Computational Biology Lab (DLab), Centro de Modelamiento Matematico (CMM), Facultad de Ciencias Fisicas y Matematicas,
Universidad de Chile,
Santiago, Chile

T. Pérez-Acle
Fundacion Ciencia para la Vida,
Zañartu 1482, Ñuñoa Santiago, Chile

T. Pérez-Acle
Centro Interdisciplinario de Neurociencias de Valparaiso (CINV),
Pasaje Harrington 287, Playa Ancha Valparaiso, Chile

P. Thomas · R. A. Tapia · C. O. Salas (✉)
Departamento de Quimica Organica, Facultad de Quimica,
P. Universidad Catolica de Chile,
Av Vicuña Mackenna 4860,
Macul- Santiago, Chile
e-mail: cosalas@uc.cl

two related ATP-dependent peptide ligases (Scheme 1): i) glutamate cysteine ligase (GCL or GSH1, EC 6.3.2.2) and ii) glutathione synthetase (GSH2, EC 6.3.2.3) [2, 3]. The GCL reaction is rate limiting and essential for the parasite as shown by RNAi experiments [4]. TcGCL activity is precisely controlled by non-allosteric feedback inhibition by glutathione, the limited availability of cellular L-Cys and the transcriptional and post-transcriptional regulation of the enzyme's expression under various physiological conditions [5, 6]. Generated glutathione, is then conjugated with spermidine by trypanothione synthetase (TryS, EC 6.1.1.9) to form trypanothione (T(SH)2), the central thiol that delivers electrons for the synthesis of DNA precursors, the detoxification of hydroperoxides and other trypanothione-dependent pathways [7–9].

GCLs sequences can be classified in three groups: i) sequences primarily from gamma-proteobacteria; ii) sequences from non-plant eukaryotes; and iii) sequences primarily from alpha-proteobacteria and plants. Although sequence identities between groups are insignificant, some conserved sequence motifs are found, suggesting distant phylogenetic relationship [10]. Recently, the crystal structures of *Saccharomyces cerevisiae* GCL (ScGCL) in complex with BSO and GSH were solved at 2.20 Å and 2.50 Å resolution (pdb ids 3LVV and 3LVW, respectively) [11]. Despite their low sequence identity (<10 %), ScGCL shares significant structural similarity with *Brassica juncea* (BjGCL) and *Escherichia coli* GCL (EcGCL). Both proteins were solved in complex with BSO (pdb id 2GWC and pdb id 1VA6, respectively) [12–14]. All these enzymes provide a source of structural insights to identify main protein-ligand interactions for buthionine sulfoximine (BSO) and other analogs. In all these cases, the inhibitors bind on the bottom of the catalytic domain comprised by six anti-parallel β-strands that form a partial barrel with a funnel-like shaped internal cavity (Fig. 1). The sequence of the small variable domain changes widely among GCL family members; sequence analysis revealed that there are no conserved regions corresponding to these sequences among family members of mechanistically related glutamine synthetase [14].

In light of its central role in the essential glutathione and trypanothione metabolism, GCL has been studied as a target for the design and identification of novel analogs of BSO [15–18], an inhibitor of GCL and effective GSH-depleting agent, which have shown to prolongs survival of mice infected with *Trypanosoma brucei* and increases the trypanocidal activity

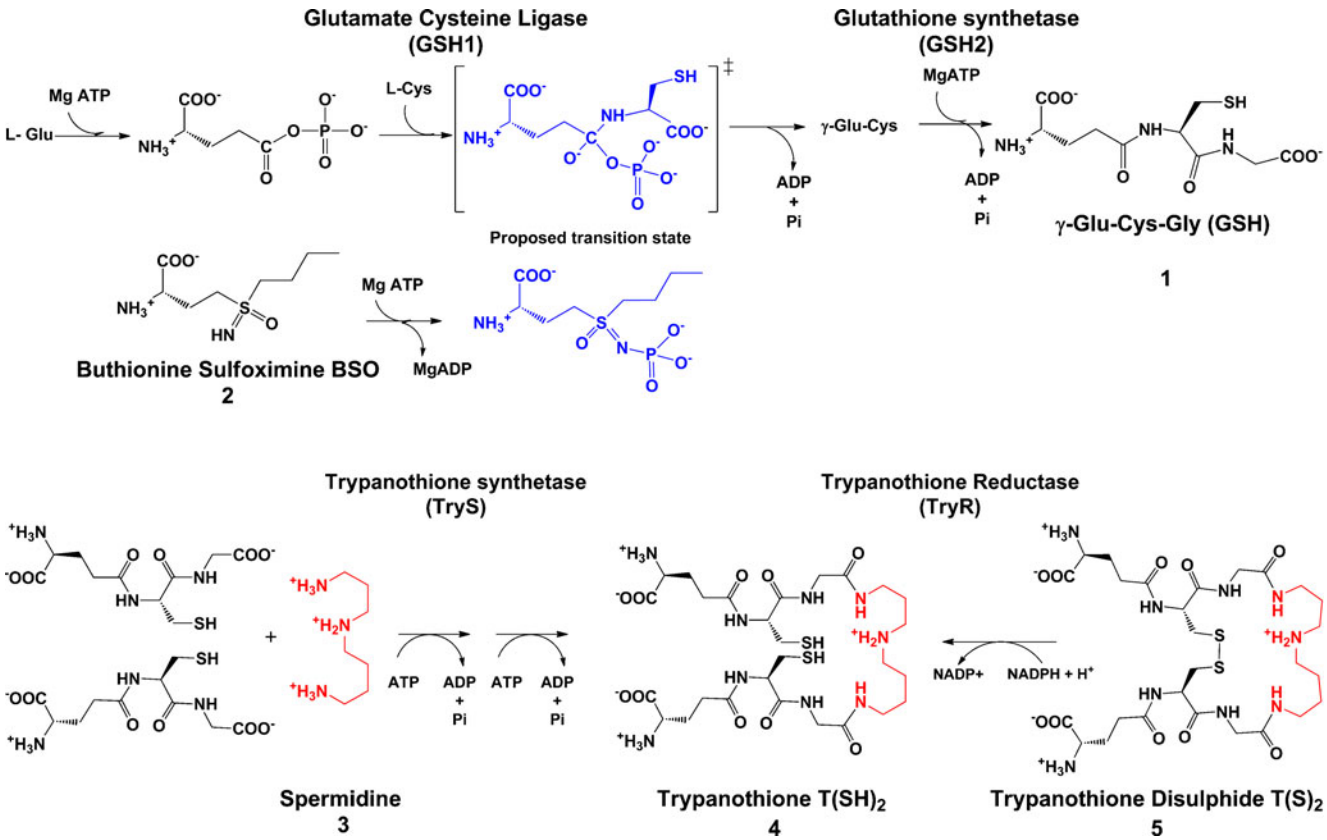

Scheme 1 Biosynthetic pathways for Glutathione and Trypanothione in *Trypanosoma cruzi*

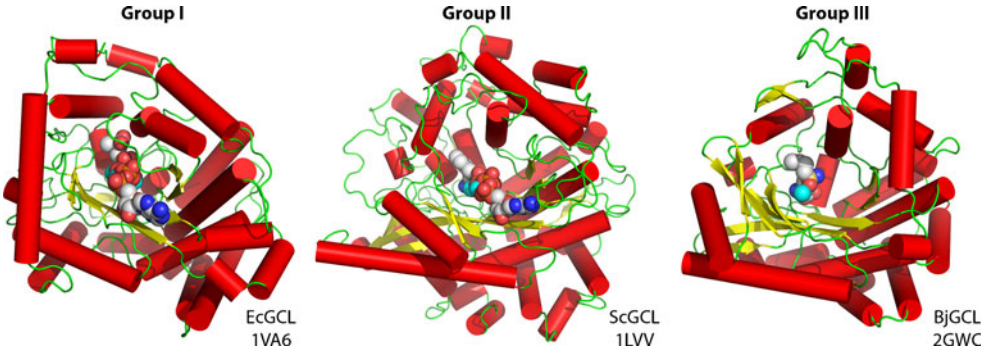

Fig. 1 Topology of GCLs proteins. Class I GCLs are mainly bacterial, class II eukaryotic and class III mostly plant homologues. Co-crystallized ligands and cofactor metals are shown as spheres for comparison

of Nifurtimox and Benznidazole against *Trypanosoma cruzi* [19–22]. Unfortunately, structure-activity relationships considering GSH or sulfoximine-based transition state analogues have not been assessed for *T. cruzi* GCL. However, some efforts have been conducted for GCL homologues present in *E. coli*, *T. brucei*, rat and human [23–29].

In this work, we report the comparative modeling of TcGCL and the investigation of its interaction with GSH, the identification of the preferred binding modes, and the development of structure-based pharmacophore models suitable for the design and identification of novel chemical entities targeting TcGCL.

Materials and methods

Molecular modeling

The molecular model of TcGCL was constructed using Modeller [30] as implemented in the Protein Modeling module of Discovery Studio 2.1 (Accelrys Inc., San Diego, CA). The sequence of TcGCL (Uniprot entry O77252) [31] was aligned with that of the class II *Saccharomyces cerevisiae* GCL in complex with GSH, solved at 2.5Å of resolution (pdb id 3LVW and Uniprot entry P32477) [11]. Due to the lack of an appropriate template, residues 214–283 of TcGCL were not included in the model. The copy ligand function was used to model the crystallographic position of GSH. Secondary structure restrains were applied in the following segments according to PCI-SS secondary structure prediction [32]: W13-T40 helix, K81-D86 helix, S113-S130 helix, S227-A238 helix, P444-K463 helix, Y492-R496 strand, P507-S511 strand, K522-V533 helix, and E587-E623 helix. A total of 100 models were constructed and the best model according to Modeller internal DOPE score was subjected to a loop refinement protocol that was applied to the P240-H248 zone. Twenty-five different loop conformations were constructed and the best-generated loop variant model according to CHARMM energies was subjected to a molecular minimization protocol using the CHARMM 22 force-field [33]. The protocol consisted of 5000 steps of steepest descent method followed by 10,000 steps of conjugate gradient method to reach a final root-mean square (RMS) gradient of 0.001 kcal mol^{-1} $Å^{-1}$. The overall quality of the final model was assessed by Ramachandran plot analysis using the RAMPAGE server [34] and Profiles-3D analysis [35]. Additional quality model assessments were performed using the ProSA-web [36], QProt [37] and SAVES (http://nihserver.mbi.ucla.edu/) servers. Binding site search was performed in Discovery Studio 2.1 with default parameters. DelPhi software was used to calculate the spatial distribution of electrostatic potential on protein atoms, using a two-dielectric implicit solvent model and the finite difference method to solve the Poisson-Boltzmann equation. The dielectric constant used for protein was 2 and 80 for the solvent [38].

Molecular dynamics (MD) simulation

The simulated periodic cells were constructed using VMD v1.9 [39] and comprised the TcGCL model alone and the TcGCL model plus the GSH molecule. The models were solvated in a water box, keeping at least 18 Å between every protein atom and the cell boundaries. Both systems were neutralized by randomly placing 16 and 17 Na^{+} ions for TcGCL and TcGCL-GSH respectively. The final dimensions of the periodic cells were 95x106x91 Å comprising a total of ~86,300 atoms. The systems were minimized and subjected to MD for 0.2 ns with the protein fixed. The proteins were then released keeping alpha carbons and side-chain non-hydrogen atoms constrained with a force constant of 20 and 5 kcal mol^{-1} $Å^{-2}$ respectively. The full systems were then minimized and a slow relaxation procedure was performed in which the constraint applied to alpha carbon atoms and side-chain non-hydrogen atoms of the proteins were decreased at a rate of 0.5 kcal mol^{-1} ps^{-1} until no constraints were applied. Subsequently, 12 ns of unconstrained NPT-MD simulation were performed with the first 2 ns considered as equilibration and the last 10 ns considered for analysis. The MD program NAMD [40] with CHARMM22 force field

corrected by CMAP for proteins [41, 42] and TIP3P for water were used for the simulation [43]. Periodic boundary conditions were imposed and the particle mesh Ewald method [44, 45] was used for electrostatic forces calculation. Constant temperature (300K) and pressure (1 atm) were maintained by using Langevin dynamics [46]. The SHAKE algorithm [47] was applied to constrain the lengths of all bonds that involve hydrogen allowing the use of a 2 fs integration timestep. MD trajectory analyses were performed with VMD v1.9 to calculate the Cα root-mean square deviation (Cα−RMSD) and the residue wise Cα root-mean square fluctuation (Cα−RMSF), for each system.

RMSD clustering and binding mode selection

To generate a reduced set of structures that represent the dynamical behavior of the GSH binding site of TcGCL, a root-mean-square deviation (RMSD) conformational clustering was performed to reduce the structural redundancy in the MD ensemble. Two hundred receptor conformations were extracted from the 10 ns MD trajectory, one every 50 ps. The structures of the trajectory were superimposed using all α-carbon atoms to remove overall rotation and translation in order that subsequent RMSD calculations could focus on the internal conformational variability of the protein. A hierarchical clustering procedure was performed with the WORDOM (v0.21) software [48] based on a subset of 15 residues located within a 5 Å radius from the center of mass of the GSH molecule during the MD-simulation (Residues: 55 93 94 179 180 183 256 260 262 264 311 335 412 and 415). These residues were grouped into clusters of similar configurations using the atom-positional RMSD for all atoms (including side chains and hydrogen) as the similarity criterion. A cutoff of 1.5 Å was chosen. The central member within each cluster, i.e., the structure having the smallest RMSD to all other structures, was chosen as the representative structure.

Binding energy calculations and pharmacophore hypotheses generation

Each cluster representative structure was minimized to convergence using 5000 steps of steepest descent method followed by 10,000 steps of conjugate gradient method to reach a final root-mean square (RMS) gradient of 0.001 kcal mol^{-1} Å. The Ludi 2 empirical scoring function was used to estimate the binding energy and the individual energy descriptors that contribute to the score. For each minimized structure, a structure-based pharmacophore hypothesis was generated with LigandScout v3.01 (Inteligand GmbH, Vienna, Austria). Chemical features perception was performed using default parameters.

Results and discussion

Comparative modeling

The *Saccharomyces cerevisiae* glutamate cysteine ligase ScGCL in complex with glutathione (3LVW) was identified as a suitable template for modeling using the sequence search facility in the Protein Data Bank [49]. For residues 214–283 of TcGCL, no suitable template structure could be identified. The initial alignment obtained from the PDB-BLAST search was manually corrected by inserting or removing gaps. After several rounds of comparative modeling, where we evaluated the impact of the alignment corrections on the secondary structure, a set of constrains were used to preserve the length of predicted secondary structure elements (see methods). The final alignment between TcGCL and ScGCL shows a 32.7% and 52.2% sequence identity and sequence similarity respectively (Fig. 2). According to STRIDE web-server [50], the secondary structure is composed of 18 α-helices, 12 extended β-sheets and two 3–10 helices. In contrast with other GCLS such as EcGCL (1 disulfide bridge) and BjGCL (3 disulfide bridges), ScGCL has no disulfide bridges. It is important to note that *Trypanosoma brucei* GCL, the best-characterized trypanosome GCL, has no reported disulfides bridges. For these reasons, no disulfide bridges were included in our model. Although DiANNA server [51] predicts 2 disulfide bridges between cysteines 72–196 (score 0.95909) and 241–255 (Score 0.82679), analysis of TcGCL model shows that the first pair is far away in the structure (distance ~18 Å) and the second pair is not present in our model, which lacks the portion containing these residues. The model is in agreement with mutagenesis data for *Trypanosoma brucei* GCL (TbGCL), to which TcGCL has a 67.7% and 81.6% sequence identity and sequence similarity respectively [2, 24] (Fig. S1). The resulting TcGCL minimized model was superimposed with ScGCL and a root-mean square deviation (RMSD) of 0.8 Å based on alpha carbon atoms (Cα-RMSD) of 600 equivalent residues was obtained (Fig. 3a). The final TcGCL structure contains 623 residues, of which 97.3% of them were found in allowed region and 2.7% in the outlier region of the Ramachandran plot according to the RAMPAGE server evaluation (Fig. 3b). The Profile-3D score was also computed to measure the compatibility of the protein model with its sequence, using a 3D profile. A ten residues window size for smoothing and the Kabsch-Sander secondary structure were used. A compatibility score of 203.35 with a maximum expected score of 286.07 was obtained for the model. These values compare well with the profile and score of 277.88 for the template structure ScGCL (Fig. 3c). The results obtained from the SAVES server for the Ramachandran Plot

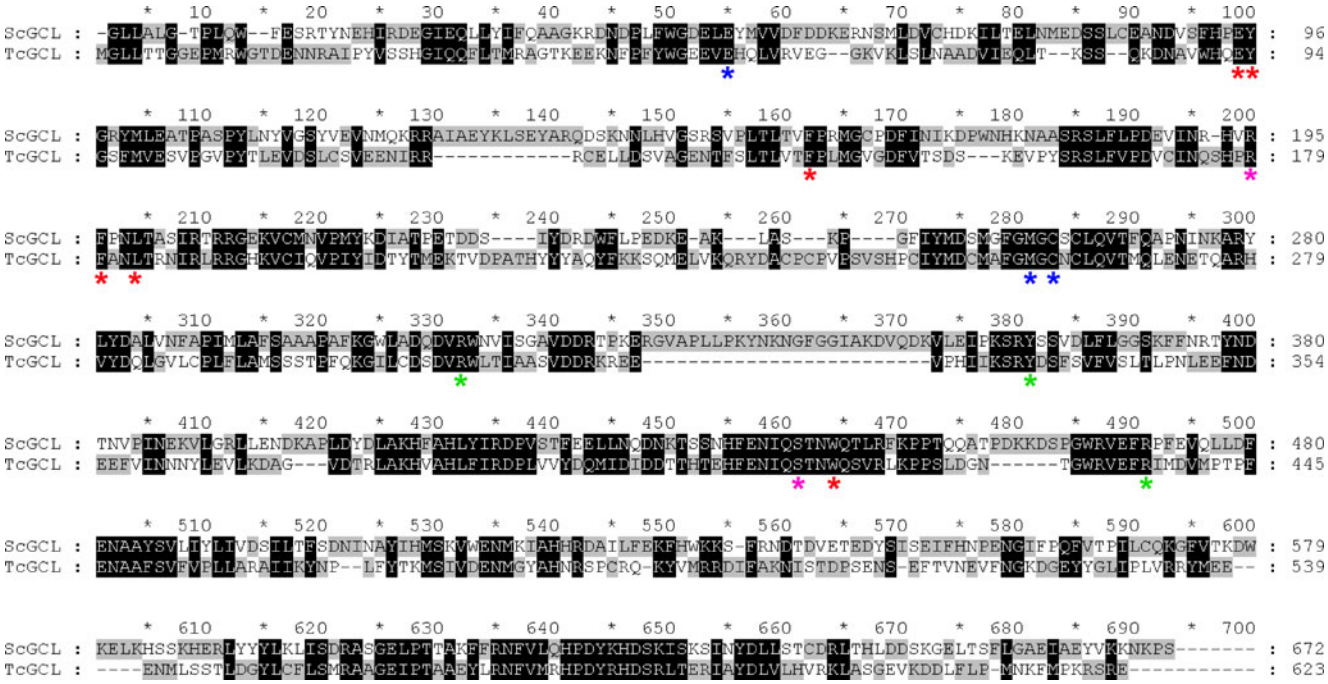

Fig. 2 Sequence alignment between TcGCL and template ScGCL proteins. Residues interacting with GSH are marked with blue and red, green and magenta asterisks for Glu-COO^-, Glu-NH_3^+, Cys and Gly binding sites respectively

(PROCHECK) and Verify 3D profiles using a window size of 21 residues for smoothing compared well with those obtained with Rampage and Profile3D respectively (Fig. S2). The ProSA-web server quality assessment provides a Z-score of −10.73 and −8.43 for the template and model structure respectively (Fig. S3). This result indicates that the TcGCL

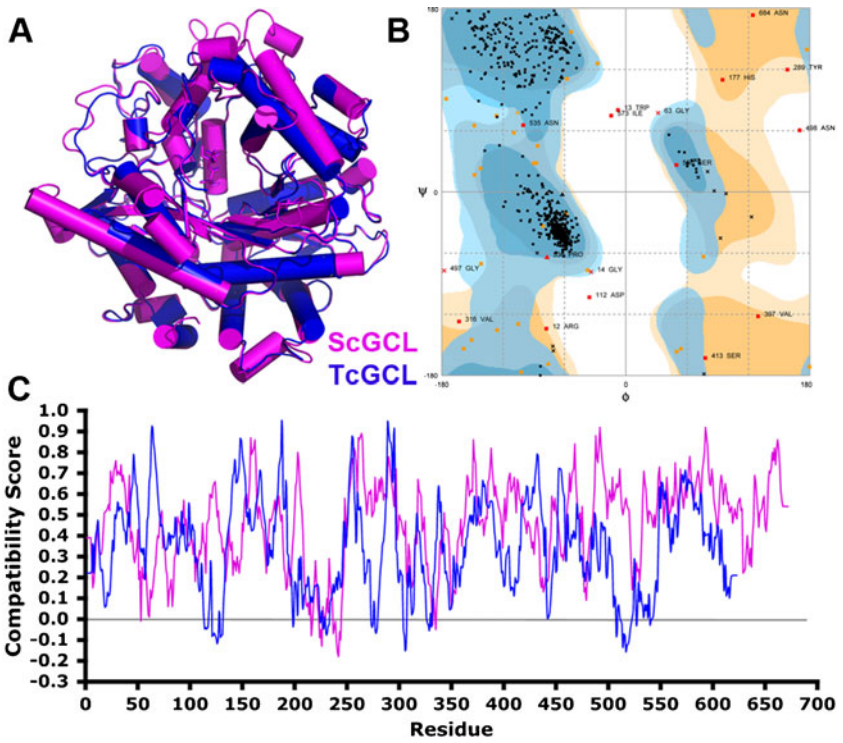

Fig. 3 Comparative modeling of TcGCL (**a**) Structural superposition between TcGCL model and template. (**b**) Ramachandran plot from RAMPAGE, (**c**) Profiles-3D plot of TcGCL model and template structure

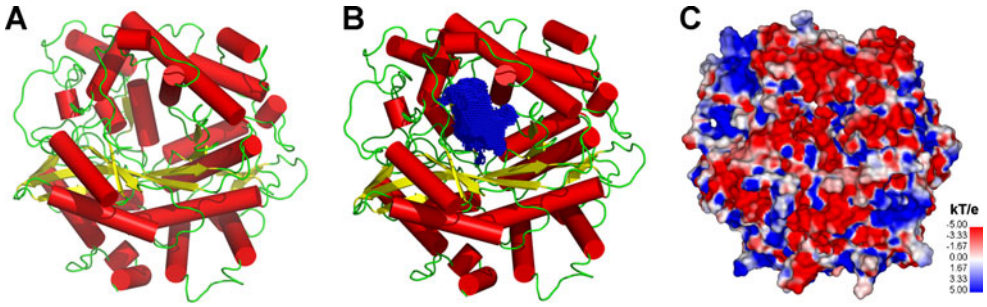

Fig. 4 From left to right. Topology, binding site cavity and electrostatic potential surface of the obtained TcGCL model

model is of similar quality as equivalent sized X-ray structures. The ProQ neural network provided an LGscore of 5.726 and 6.464 for the TcGCL model and the template structure respectively. This method considers that models with LGscore>4 are extremely good. All these results suggest that the fold of the TcGCL model is reliable and the model is suitable for further analysis and studies. Figure 4a shows the 3D-structure of the minimized TcGCL-GSH model. A 726 Å^3 cavity was identified with the binding site analysis module of DS2.1 (Fig. 4b) and a highly electronegative

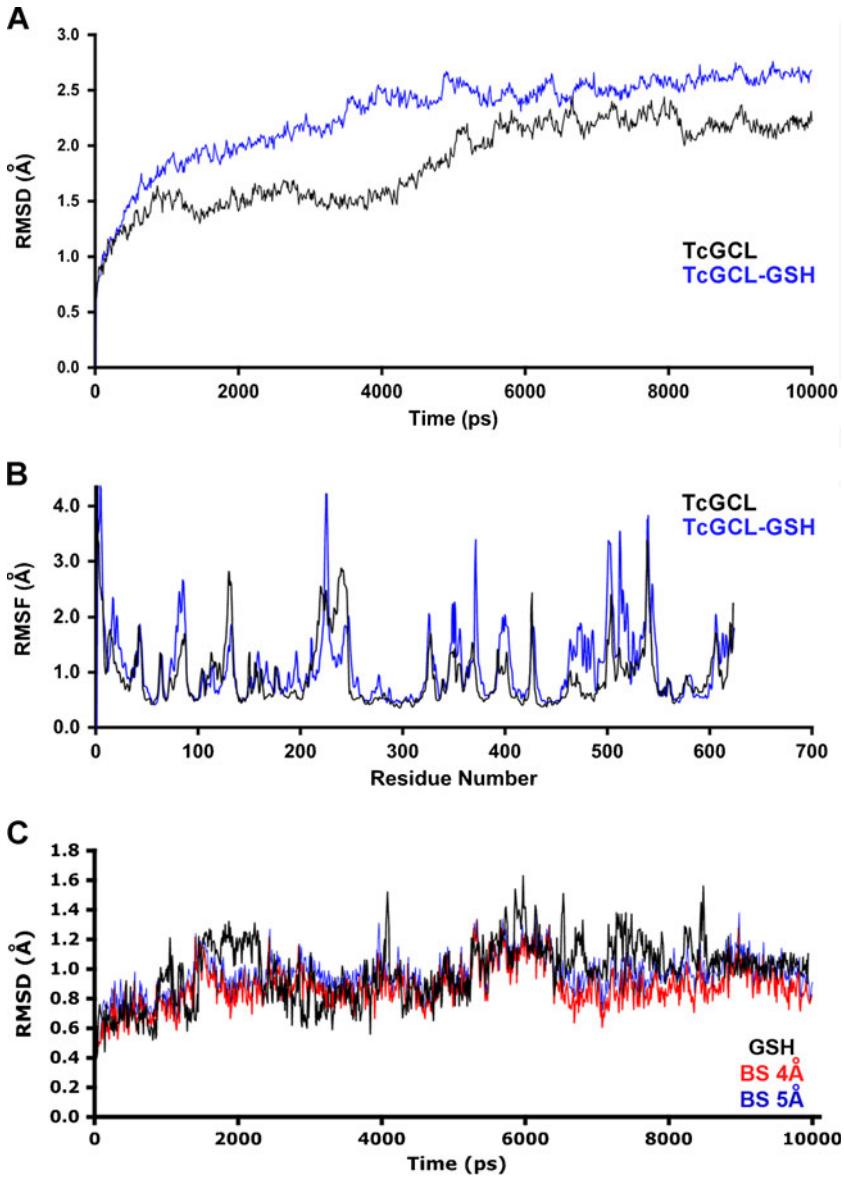

Fig. 5 (**a**) Cα-RMSD of TcGCL and TcGCL-GSH complex during the MD, (**b**) Cα-RMSF of TcGCL and TcGCL-GSH complex during the MD. (**c**) RMSD of GSH, and α-carbons from residues within 4 and 5 Å from GSH during MD

GSH binding site was identified by the Delphi spectrum (Fig. 4c).

Molecular dynamics simulations

TcGCL is thought to be biologically functional as a monomer [52], and can be feedback inhibited by GSH. In order to study the TcGCL-GSH complex stability, a 10 ns molecular dynamics simulation was performed. Figure 5a shows the alpha carbon RMSD plot using the first frame of the production stage of the simulation as reference for the TcGCL-GSH and using the TcGCL alone as a control. The proteins reach a stable equilibrated state after 4 ns of simulation, with an average Cα-RMSD value of 2.27± 0.38 Å. The Cα root mean square fluctuation (RMSF) plot for each residue during the simulation was calculated to identify the most mobile residues, all of which are located far from the GSH binding site (Fig. 5b). The calculated RMSDs for GSH (average 0.99±0.20 Å) and for the residues surrounding it at 4 and 5Å (average 0.89±0.14 and 0.96±0.13 Å, respectively) show that the binding site is fairly rigid but some movement can be detected. As expected, correlated deviations are observed between GSH and the binding site (Fig. 5c). To further characterize this behavior, the binding pattern between GSH and relevant conserved binding site residues was followed during simulation and analyzed. The H-bond pattern for which distances were measured is shown in Fig. 6a. As shown in Fig. 6b, for the glutamate carboxylate group or motif of GSH (Glu:COO^-) distances between R381:NE/Glu:OT2, Y405:OH/Glu:OT1 and R506:NH2/Glu:OT1 are within hydrogen bond distance, except for the C334:SG/Glu:OT2 interaction, with average values of 2.82±0.13, 2.60±0.09, 2.73±0.11 and 4.09±0.36 Å, respectively. This result is in agreement with mutagenesis data that shows that the equivalent residue in TbGCL enzyme (C319) has no significant effect on the specific activity of the enzyme [53]. For the charged amino moiety of GSH (Glu:NH_3^+), the distance to E55:OE1, C332:O and M330:O are within hydrogen bond distances with average values of 2.68±0.09, 2.74±0.12 and 3.00±0.26 Å, respectively. In particular the interaction with the main-chain carbonyl of M330 is non-water mediated in contrast to the corresponding interaction with the M262 residue in ScGCL. For the cysteine residue of GSH distances E93:OE1/Cys:NH, E93:OE2/Cys:NH and W485:NE1/Cys:O are within hydrogen bond distance, with average values of 3.32±0.28, 2.84±0.17 and 3.20±0.37 Å, respectively. Finally, for the glycine residue of GSH the measured distances E93:OE2/Gly:NH, R179:NH/Gly:OT2, R179:NH2/Gly:OT1 and R179:CZ/Gly:C, with average distances of 3.17±0.52, 3.63±1.00, 4.04±1.21 and 4.31± 0.69 Å, respectively, are consistent with a hydrogen bond with E93, and a transient double salt bridge between R179 and the terminal carboxylate observed around 1.5-2.5 ns of

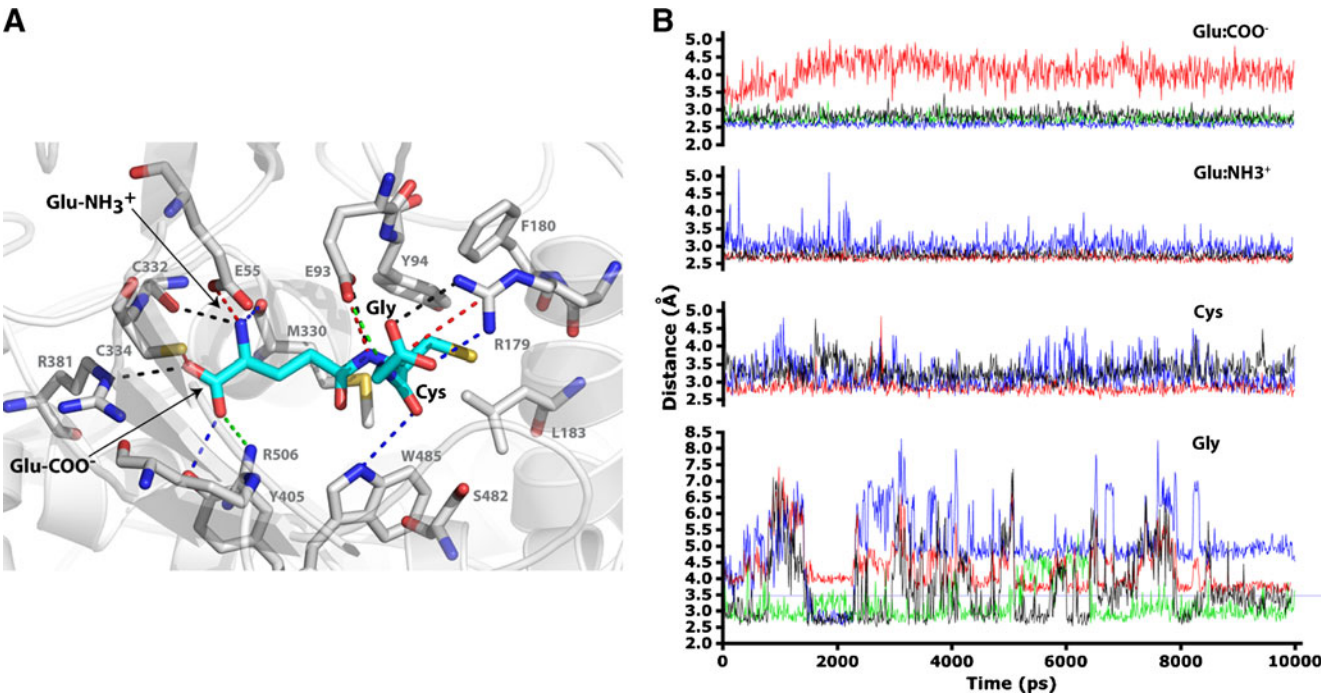

Fig. 6 (**a**) Snapshot of the averaged TcGCL-GSH complex during simulation, water molecules are not shown for clarity. (**b**) Binding site H-bond interaction distances between several GSH atoms and the Glu, Cys and Gly binding sites residues during MD. Distance colors are shown as in panel A for each zone

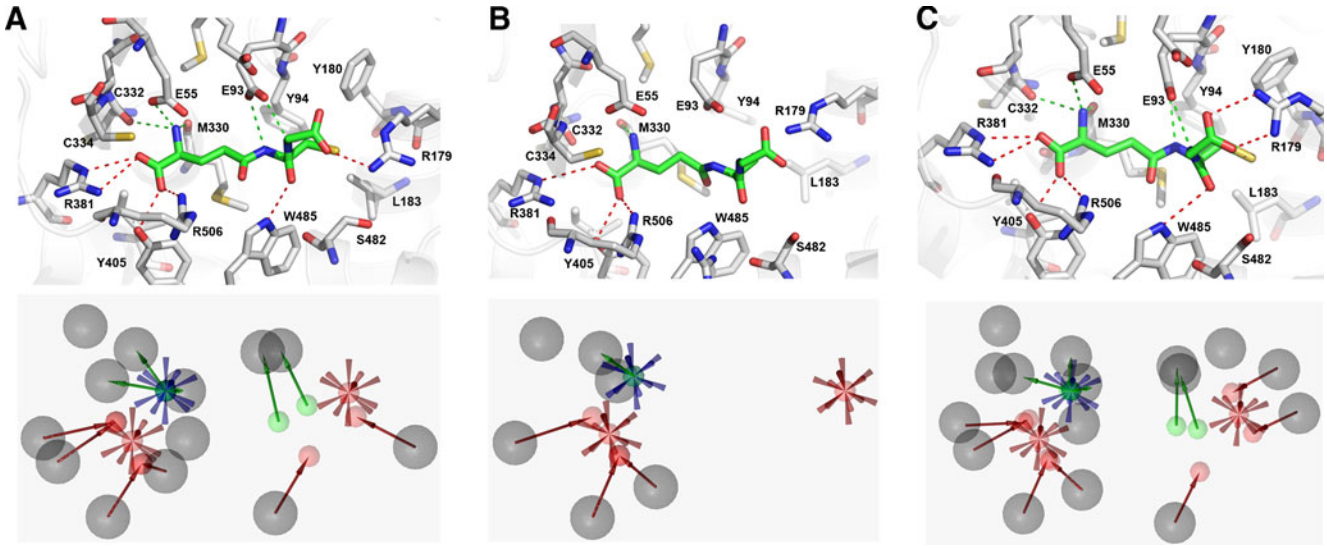

Fig. 7 Representative binding modes for GSH during simulation obtained by RMSD clustering of the binding site residues and their corresponding pharmacophore models for GSH interaction binding mode. (**a**) Cluster 1 (24%), (**b**) Cluster 2 (7%), and (**c**) Cluster 3 (69%). Gray exclusion spheres represent the sterical circumference of the protein, red vectors are H-bond acceptor and green vectors H-bond donors. Spiked red and blue spheres are negative and positive ionizable groups

simulation, which can be explained by the high flexibility of the terminal glycine residue of GSH. These results reveal that the GSH binding site has a rigid and a flexible zone. The rigid zone comprises the glutamate zwitterion binding residues and the cysteine counterparts, and the flexible zone is mainly located within the terminal carboxy group of glycine.

RMSD clustering and binding mode selection

To identify the preferred GSH binding modes suggested by trajectory analysis, an RMSD conformational clustering based on the GSH binding site was performed on a set of 200 snapshots separated by 50 ps taken from the trajectory, in order to reduce structural redundancy in the MD ensemble. Using a 1.5 Å cut-off, we identified three clusters from which the structure, from each cluster having the smallest RMSD to all other structures within the cluster was selected as the representative structure as shown in Fig. 7. Cluster 1 (Fig. 7a) contains 48 structures and represents a 24% of occurrence during the MD, cluster 2 (Fig. 7b) contains only 14 structures representing the 7%, and cluster 3 (Fig. 7c) contains 138 structures and account for the last 69%.

Binding energy calculations and pharmacophore hypotheses generation

Individual components of the binding energy estimated using the Ludi 2 empirical scoring function for each representative structure show that ionic, lipophilic, and H-bond interactions display similar energy contribution (Table 1). A comparison of the structure based pharmacophore models suggest that drop in binding affinity can be explained by the loss of key H-bond and ionic interactions between GSH and TcGCL residues E55, E93, R179, C332 and W485. Several of these residues have been reported as essential for the binding and stabilization of metal and L-Glu positioning for further metal-dependent complexation with L-Cys [2]. In particular Glu93, a metal binding determinant, plays an important role by anchoring both GSH-Cys and GSH-Gly amino groups, making this residue less available to metal binding. Aliphatic interactions between the carbon chain of GSH-Glu and the side-chain of I385, and the interactions of the GSH-Cys side-chain with the Cys binding site composed of the side-chain of residues L173, R179, F180, M330 and W485, appears to account for the Lipo component in binding energy. R179 is highly conserved between GCLs and R179 to Ala alters the

Table 1 Energy contribution of GSH binding modes clusters, according to Ludi 2 scoring function

Cluster	ΔG (kcal/mol)	ΔG H-bond	ΔG Lipo	ΔG Ionic	ΔG Rot
1	−8.237	−2.550	−3.137	−3.832	1.964
2	−5.100	−1.146	−2.946	−2.291	1.964
3	−8.673	−3.327	−3.027	−3.600	1.964

active site and effects the substrate dependencies [24]. In our model R179 plays a role highly relevant for GSH binding, acting as a lid that allow the transition between a high and a low affinity state through the formation of a double salt-bridge with the carboxylate group of GSH-Gly. Thus, targeting the residues involved in these relevant interactions seems a reasonable strategy for the development of GCLs modulators.

Conclusions

In this study, we present the first molecular model for *Trypanosoma cruzi* glutamate cysteine ligase TcGCL. Analysis of the results of the comparative modeling procedure and MD simulations indicated that the theoretical predictions and obtained fold is consistent with the known set of experimental results available for *Trypanosoma* GCL and other homologues. Molecular dynamics simulations and binding energy contribution analyses highlight the relevant forces involved in the GSH binding, and identify E93 and R179 with putative roles as anchor and switch key residues that could explain the differential binding mode of GSH within the TcGCL active site. The prevalent binding modes and their pharmacophore-derived models provide a source for structure-based design of new GCL inhibitors.

Acknowledgments The authors would like to thank Fondo Nacional de Desarrollo Científico y Tecnológico (FONDECYT, Chile) project Nº 11085027 to COS for financial support. RAT acknowledges Programa Bicentenario de Ciencia y Tecnología del Proyecto de Inserción (PSD70). TPA acknowledge to Proyectos de Financiamiento Basal PFB03 and PFB16, and to Millenium Institute Centro Interdisciplinario de Neurociencias de Valparaíso (CINV). Molecular dynamics simulations were performed at the National Laboratory for High Performance Computing (NLHPC ECM-02) supercomputing infrastructure: Powered@NLHPC. CFL, RAS and PT are PhD fellows from Comisión Nacional de Investigación Científica y Tecnológica (CONICYT, Chile).

References

1. Moncayo A, Silveira AC (2009) Current epidemiological trends for Chagas disease in Latin America and future challenges in epidemiology, surveillance and health policy. Mem Inst Oswaldo Cruz 104(Suppl 1):17–30
2. Abbott JJ, Pei J, Ford JL, Qi Y, Grishin VN, Pitcher LA, Phillips MA, Grishin NV (2001) Structure prediction and active site analysis of the metal binding determinants in gamma -glutamylcysteine synthetase. J Biol Chem 276:42099–42107
3. Brekken DL, Phillips MA (1998) Trypanosoma brucei gamma-glutamylcysteine synthetase. Characterization of the kinetic mechanism and the role of Cys-319 in cystamine inactivation. J Biol Chem 273:26317–26322
4. Huynh TT, Huynh VT, Harmon MA, Phillips MA (2003) Gene Knockdown of γ-Glutamylcysteine Synthetase by RNAi in the Parasitic Protozoa Trypanosoma brucei Demonstrates That It Is an Essential Enzyme. J Biol Chem 278:39794–39800
5. Krzywanski DM, Dickinson DA, Iles KE, Wigley AF, Franklin CC, Liu RM, Kavanagh TJ, Forman HJ (2004) Variable regulation of glutamate cysteine ligase subunit proteins affects glutathione biosynthesis in response to oxidative stress. Arch Biochem Biophys 423:116–125
6. Hiratake J (2005) Enzyme inhibitors as chemical tools to study enzyme catalysis: rational design, synthesis, and applications. Chem Rec 5:209–228
7. Ariyanayagam MR, Oza SL, Mehlert A, Fairlamb AH (2003) Bis (glutathionyl)spermine and other novel trypanothione analogues in Trypanosoma cruzi. J Biol Chem 278:27612–27619
8. Oza SL, Tetaud E, Ariyanayagam MR, Warnon SS, Fairlamb AH (2002) A single enzyme catalyses formation of Trypanothione from glutathione and spermidine in Trypanosoma cruzi. J Biol Chem 277:35853–35861
9. Wyllie S, Oza SL, Patterson S, Spinks D, Thompson S, Fairlamb AH (2009) Dissecting the essentiality of the bifunctional trypanothione synthetase-amidase in Trypanosoma brucei using chemical and genetic methods. Mol Microbiol 74:529–540
10. Copley SD, Dhillon JK (2002) Lateral gene transfer and parallel evolution in the history of glutathione biosynthesis genes. Genome Biol 3:research0025
11. Biterova EI, Barycki JJ (2010) Structural basis for feedback and pharmacological inhibition of Saccharomyces cerevisiae glutamate cysteine ligase. J Biol Chem 285:14459–14466
12. May MJ, Leaver CJ (1994) Arabidopsis thaliana gamma-glutamylcysteine synthetase is structurally unrelated to mammalian, yeast, and Escherichia coli homologs. Proc Natl Acad Sci USA 91:10059–10063
13. Hothorn M, Wachter A, Gromes R, Stuwe T, Rausch T, Scheffzek K (2006) Structural basis for the redox control of plant glutamate cysteine ligase. J Biol Chem 281:27557–27565
14. Hibi T, Nii H, Nakatsu T, Kimura A, Kato H, Hiratake J, Oda J (2004) Crystal structure of gamma-glutamylcysteine synthetase: insights into the mechanism of catalysis by a key enzyme for glutathione homeostasis. Proc Natl Acad Sci USA 101:15052–15057
15. Hamilton D, Wu JH, Batist G (2007) Structure-based identification of novel human gamma-glutamylcysteine synthetase inhibitors. Mol Pharmacol 71:1140–1147
16. Griffith OW (1982) Mechanism of action, metabolism, and toxicity of buthionine sulfoximine and its higher homologs, potent inhibitors of glutathione synthesis. J Biol Chem 257:13704–13712
17. Griffith OW, Meister A (1979) Potent and specific inhibition of glutathione synthesis by buthionine sulfoximine (S-n-butyl homocysteine sulfoximine). J Biol Chem 254:7558–7560
18. Griffith OW, Anderson ME, Meister A (1979) Inhibition of glutathione biosynthesis by prothionine sulfoximine (S-n-propyl homocysteine sulfoximine), a selective inhibitor of gamma-glutamylcysteine synthetase. J Biol Chem 254:1205–1210
19. Faundez M, Pino L, Letelier P, Ortiz C, Lopez R, Seguel C, Ferreira J, Pavani M, Morello A, Maya JD (2005) Buthionine sulfoximine increases the toxicity of nifurtimox and benznidazole to Trypanosoma cruzi. Antimicrob Agents Chemother 49:126–130
20. Moncada C, Repetto Y, Aldunate J, Letelier ME, Morello A (1989) Role of glutathione in the susceptibility of Trypanosoma cruzi to drugs. Comp Biochem Physiol C 94:87–91
21. Repetto Y, Opazo E, Maya JD, Agosin M, Morello A (1996) Glutathione and trypanothione in several strains of Trypanosoma cruzi: effect of drugs. Comp Biochem Physiol B Biochem Mol Biol 115:281–285
22. Maya JD, Cassels BK, Iturriaga-Vasquez P, Ferreira J, Faundez M, Galanti N, Ferreira A, Morello A (2007) Mode of action of natural and synthetic drugs against Trypanosoma cruzi and their interac-

tion with the mammalian host. Comp Biochem Physiol A Mol Integr Physiol 146:601–620
23. Harvison PJ, Kalman TI (1992) Synthesis and biological activity of novel folic acid analogues: pteroyl-S-alkylhomocysteine sulfoximines. J Med Chem 35:1227–1233
24. Abbott JJ, Ford JL, Phillips MA (2002) Substrate binding determinants of Trypanosoma brucei gamma-glutamylcysteine synthetase. Biochemistry 41:2741–2750
25. Janowiak BE, Griffith OW (2005) Glutathione synthesis in Streptococcus agalactiae. One protein accounts for gamma-glutamylcysteine synthetase and glutathione synthetase activities. J Biol Chem 280:11829–11839
26. Jez JM, Cahoon RE, Chen S (2004) Arabidopsis thaliana glutamate-cysteine ligase: functional properties, kinetic mechanism, and regulation of activity. J Biol Chem 279:33463–33470
27. Huynh TT, Huynh VT, Harmon MA, Phillips MA (2003) Gene knockdown of gamma-glutamylcysteine synthetase by RNAi in the parasitic protozoa Trypanosoma brucei demonstrates that it is an essential enzyme. J Biol Chem 278:39794–39800
28. Ashida H, Sawa Y, Shibata H (2005) Cloning, biochemical and phylogenetic characterizations of gamma-glutamylcysteine synthetase from Anabaena sp. PCC 7120. Plant Cell Physiol 46:557–562
29. Drew R, Miners JO (1984) The effects of buthionine sulphoximine (BSO) on glutathione depletion and xenobiotic biotransformation. Biochem Pharmacol 33:2989–2994
30. Sali A, Blundell TL (1993) Comparative protein modelling by satisfaction of spatial restraints. J Mol Biol 234:779–815
31. The UniProt Consortium (2009) The Universal Protein Resource (UniProt) 2009. Nucl Acids Res 37:D169–D174
32. Green JR, Korenberg MJ, Aboul-Magd MO (2009) PCI-SS: MISO dynamic nonlinear protein secondary structure prediction. BMC Bioinforma 10:222
33. Brooks BR, Bruccoleri RE, Olafson BD, States DJ, Swaminathan S, Karplus M (1983) CHARMM: A program for macromolecular energy, minimization, and dynamics calculations. J Comput Chem 4:187–217
34. Lovell SC, Davis IW, Arendall WB 3rd, de Bakker PI, Word JM, Prisant MG, Richardson JS, Richardson DC (2003) Structure validation by Calpha geometry: phi, psi and Cbeta deviation. Proteins 50:437–450
35. Luthy R, Bowie JU, Eisenberg D (1992) Assessment of protein models with three-dimensional profiles. Nature 356:83–85
36. Wiederstein M, Sippl MJ (2007) ProSA-web: interactive web service for the recognition of errors in three-dimensional structures of proteins. Nucleic Acids Res 35:W407–W410
37. Wallner B, Elofsson A (2003) Can correct protein models be identified? Protein Sci 12:1073–1086
38. Honig B, Nicholls A (1995) Classical electrostatics in biology and chemistry. Science 268:1144–1149
39. Humphrey W, Dalke A, Schulten K (1996) VMD: Visual molecular dynamics. J Mol Graph 14:33–38
40. Phillips JC, Braun R, Wang W, Gumbart J, Tajkhorshid E, Villa E, Chipot C, Skeel RD, Kale L, Schulten K (2005) Scalable molecular dynamics with NAMD. J Comput Chem 26:1781–1802
41. Mackerell AD Jr (2004) Empirical force fields for biological macromolecules: overview and issues. J Comput Chem 25:1584–1604
42. MacKerell AD, Bashford D, Bellott DRL, Evanseck JD, Field MJ, Fischer S, Gao J, Guo H, Ha S, Joseph-McCarthy D, Kuchnir L, Kuczera K, Lau FTK, Mattos C, Michnick S, Ngo T, Nguyen DT, Prodhom B, Reiher WE, Roux B, Schlenkrich M, Smith JC, Stote R, Straub J, Watanabe M, Wiorkiewicz-Kuczera J, Yin D, Karplus M (1998) All-Atom Empirical Potential for Molecular Modeling and Dynamics Studies of Proteins. J Phys Chem B 102:3586–3616
43. Jorgensen WL, Chandrasekhar J, Madura JD, Impey RW, Klein ML (1983) Comparison of simple potential functions for simulating liquid water. J Chem Phys 79:926–935
44. Darden T, York D, Pedersen L (1993) Particle mesh Ewald: An N [center-dot] log(N) method for Ewald sums in large systems. J Chem Phys 98:10089–10092
45. Essmann U, Perera L, Berkowitz ML, Darden T, Lee H, Pedersen LG (1995) A smooth particle mesh Ewald method. J Chem Phys 103:8577–8593
46. Feller SE, Zhang Y, Pastor RW, Brooks BR (1995) Constant pressure molecular dynamics simulation: The Langevin piston method. J Chem Phys 103:4613–4621
47. Ryckaert J-P, Ciccotti G, Berendsen HJC (1977) Numerical integration of the cartesian equations of motion of a system with constraints: molecular dynamics of n-alkanes. J Chem Phys 23:327–341
48. Seeber M, Cecchini M, Rao F, Settanni G, Caflisch A (2007) Wordom: a program for efficient analysis of molecular dynamics simulations. Bioinformatics 23:2625–2627
49. Berman HM, Westbrook J, Feng Z, Gilliland G, Bhat TN, Weissig H, Shindyalov IN, Bourne PE (2000) The Protein Data Bank. Nucleic Acids Res 28:235–242
50. Frishman D, Argos P (1995) Knowledge-based protein secondary structure assignment. Proteins 23:566–579
51. Ferre F, Clote P (2005) DiANNA: a web server for disulfide connectivity prediction. Nucleic Acids Res 33:W230–W232
52. Lueder DV, Phillips MA (1996) Characterization of Trypanosoma brucei γ-Glutamylcysteine Synthetase, an Essential Enzyme in the Biosynthesis of Trypanothione (Diglutathionylspermidine). J Biol Chem 271:17485–17490
53. Brekken DL, Phillips MA (1998) Trypanosoma brucei Gamma-Glutamylcysteine Synthetase. J Biol Chem 273:26317–26322